

Hybrid III-V semiconductor/Silicon nanolaser

Y. Halioua^{1,2}, A. Bazin¹, P. Monnier¹, T. Karle¹, G. Roelkens²; I. Sagnes¹, R. Raj¹ and F. Raineri^{1,3}

¹Laboratoire de Photonique et de Nanostructures, CNRS-UPR20, Route de Nozay, 91460 Marcoussis, France

²Photonics Research Group, Department of Information Technology, Ghent University, B-9000 Ghent, Belgium

³Université Paris Denis Diderot, 75205 Paris, France

ABSTRACT:

Heterogeneous integration of III-V semiconductor compounds on Silicon on Insulator wafers is one the key technology for next generation on chip optical interconnects. Within this context the use of photonic crystals lasers represent a disruptive solution in terms of footprint, activation energy and ultrafast response. In this work, we propose and fabricate very compact laser sources integrated with a passive silicon waveguide circuitry, taking advantage of the efficient emission from III-V semiconductor photonic crystal nanocavities. Such micro sources often radiate only a fraction of their power into useful beams. Using a subjacent Silicon-On-Insulator waveguide we capture emitted light from the cavity, evanescently, and can also probe the cavity waveguide system in transmission in order to experimentally deduce the coupling factors.

During the past decades, optical devices have played a crucial role in the domain of information and communication technology, due to their ability to bring efficient solutions to data transmission and processing. Indeed, optical communications have known tremendous development, through optical fibres backed by related devices and circuits composed of light sources, optical amplifiers, wavelength multiplexers, photodetectors, etc, which have greatly revolutionized telecommunication. Increasing attention is now being devoted to optical computer-com mainly concentrated in intra- and inter-chip interconnection applications [1,2], the convergence of optics and electronics at the chip level being a necessity for the next generation processors. Here, the issues that need to be tackled are the dispatching and sorting of the mind-boggling amount of information within small footprints and above all with reduced power consumption and dissipation [3].

Thus, photonic circuits should be constituted of elements able to control perfectly the propagation of light with a view to achieve “passive” functions such as guiding and filtering as well as elements dedicated to active functions such as emission, detection, amplification, switching and a multitude of others capable of manipulating optical information at will.

In this context, it is very unlikely that only one class of material will completely answer to all needs. Silicon photonics, enhanced by III-V based optical functions is considered to be as one of the key technologies combining the best of both materials leading to highly versatile hybrid photonics platform and opening up the field to large scale photonic integration. Indeed, Silicon transparency at telecom wavelengths and the high-index contrast with silica allows the fabrication of extremely compact low-loss single mode waveguides ($\sim 2\text{dB/cm}$) [4,5] that can be used for bringing the information where it

needs to in the circuit. Of most importance, the mature complementary metal oxide semiconductor (CMOS) fabrication processing technology makes possible large-scale integration of functional optical devices, including integration with complex electronic components. However, due to its indirect electronic band gap Silicon is not the most ideal material for light emission and light control. The direct bandgap of III-V materials makes efficient stimulated emission possible, which enables the fabrication of lasers, amplifiers, detectors and modulators. These materials offer the unique possibility to obtain a tailor made electronic band structures by playing on the combinations of elements and their respective compositions, to constitute alloys. It is then possible obtain radiative transitions at the desired wavelength of operation from 0.4 μm to 20 μm . Heterogeneous integration of III-V semiconductor on Silicon on Insulator (SOI) waveguides has recently been successfully implemented to obtain laser sources [6-9], amplifiers [10], modulators[11,12] and flip-flops [13] which constitute very exciting results for further photonic integration with electronics.

In this article, the concept of hybrid Si/III-V semiconductor photonics is extended to nanophotonics. III-V Photonic crystal nanolasers are integrated and coupled to silicon on insulator waveguides circuitry. This disruptive approach allows us to obtain low threshold hybrid lasers in the telecom window with structures as small as 5 μm^2 footprint, 10 times smaller than the smallest microdisks devices demonstrated. We minutely study the evanescent wave coupling occurring as a function of the structure parameters and show that more than **90%** of the emitted light is funneled into the SOI wires.

An innovative platform: Hybrid III-V photonic crystals nanocavities on Silicon on Insulator waveguides circuitry

The hybrid structure under study is schematically represented on Fig. 1a. It is a 2 optical level structure where one level is constituted by a single mode SOI waveguide and the second one by an InP-based photonic crystal nanocavity embedding 4 InGaAsP/InGaAs quantum wells emitting at 1.55 μm . The 2 levels are separated by a low index layer (silica+benzocyclobutene) to preserve the vertical optical confinement within the SOI waveguide and the PhC cavity. The coupling mechanism is ensured by the penetration the evanescent part of the fields within the other level [14].

The chosen nanocavity is akin a so-called “wire” or “nanobeam” [15-19] cavity, which is a Fabry-Perot type cavity formed in a single mode wire waveguide (550nm width and 255nm height). The high reflectivity mirrors are constituted by a single row of holes drilled into the material. The holes radius r and the pitch of the 1D lattice a are fixed to be respectively 177.5nm and 370 nm to obtain a large high reflectivity bandwidth around 1.55 μm . The size of the 3 holes on each side of the cavity is tapered down in order to increase the quality factor by adapting the propagating guided mode to the evanescent mirror mode [20]. These cavities are particularly interesting because they can exhibit quality factors as high as 10^5 with modal volumes close to the limit of $(\lambda/2n)^3$ even when the structures are not suspended in the air which is the case in the present study. Moreover, their footprint is about 5 μm^2 , which is at least 10 times smaller than the footprint of cavities formed in a 2 dimensional lattice of holes [21]. The SOI level is made of a 220nm thick Si layer on a 2 μm SiO₂ buffer. The Si layer is etched down in stripes in order to form waveguides. The waveguides width is varied on the dye from 350nm to 550nm in step of 50nm. At their extremities, grating couplers are etched to allow coupling

with cleaved single mode optical fibres. The fabrication of the hybrid structures which is based on dye-to-dye adhesive bonding and mixed and matched deep UV/electron beam lithography is described in the Method section. The low index layer is a bilayer composed by a thin layer of BCB (80nm) and a layer of SiO₂. 3 samples are fabricated with different SiO₂ thicknesses (200nm, 300nm and 400nm). A scanning electron microscope picture of one of the fabricated structures is given on Fig.1b where a wire cavity can be seen positioned on top of a SOI waveguide. The precision of this positioning is demonstrated to be better than 30nm, which allows us to neglect the impact of the lateral offset between the two levels on the evanescent wave coupling [22].

Laser Operation

Laser emission is explored by optically pumping the wire cavities using a 800nm laser diode focused to a 20 μm^2 spot with a 10x microscope objective. The laser diode is modulated in order to obtain 40ns pulses at a 300kHz repetition rate. The emitted light is collected at the extremities of the 5mm long SOI waveguides with SMF-28 optical fibres tilted at an angle of 10° and is analysed using a spectrometer equipped with a cooled InGaAs detectors array. We plot on Fig. 2a, in log-log scale, the output peak power of the emitted light as a function of the absorbed pump peak power for a cavity length of 450nm on a 500nm wide SOI waveguide. As expected for laser emission [23], the curve is S-shaped and the threshold is found to be 17 μW . As seen on Fig. 2b, the full width at half maximum (FWHM) of the emission spectrum decreases down to 0.18nm (which corresponds to the spectrometer resolution) as the absorbed pump power is increased up to 19.5 μW . When the pump power is further increased the emission broadens due to power broadening [24]. The emission wavelength can be easily tuned by adjusting, for example, the cavity length as shown in Fig. 2c [19]. As the cavity length is increased from 400nm to 650nm, the cavities are single mode and laser emission is observed from 1565nm to 1596nm. Above 550nm, 2 peaks are observed in the emission spectra as the cavity second order mode enters the gain region. In the following, we will focus on the single mode cavities. Continuous wave laser operation is also observed by pumping the system at 1.18 μm , a wavelength corresponding to an energy right above the gap of the InGaAsP barriers of the quantum wells. Indeed, this decrease of the pump energy lowers the number of phonons emitted during the relaxation process of electron-holes pairs which are responsible for the heating [25].

Study of the coupling efficiency

One important question remains: what is the efficiency of the coupling between the III-V nanolaser and the SOI wire? In the approximation where the presence of the SOI waveguide weakly perturbs the cavity mode, the evolution of the intra-cavity electromagnetic field can be described by the coupled modes theory [26-28]. In this theory, the cavity optical losses are determined by two independent terms, one related to the intrinsic losses of the cavity, i.e. the losses in absence of the waveguide and one related to the coupling to the SOI waveguide mode. To these losses are respectively associated the quality factors Q_0 and Q_c . The coupling efficiency can then be written as:

$$\eta = \frac{\frac{1}{Q_c}}{\frac{1}{Q_c} + \frac{1}{Q_0}}$$

It is clear that, in order to obtain a large efficiency, the losses induced by the coupling to the SOI waveguide have to be much larger than the intrinsic cavity losses ($Q_c \ll Q_0$). The coupling efficiency is plotted on Fig. 3a as a function of the ratio Q_0/Q_c . Note that, at the same time, the total losses of the system (proportional to $1/Q_0 + 1/Q_c$) have to be maintained as small as possible to allow low threshold laser emission. In the following, Q_c and Q_0 are experimentally retrieved by analysing both the transmission of an optical probe as a function of the material gain and the laser characteristic.

Considering E_{in} the amplitude of electric field propagating in the SOI waveguide incoming in the cavity as indicated in the schematics of our system given in Fig. 3b and using the coupled-mode theory, the evolution of the intra cavity field amplitude E_{cav} in presence of optical gain writes:

$$\frac{dE_{cav}}{dt} = \left(j\omega_0 - \frac{1}{\tau_0} - \frac{1}{\tau_c} + \frac{1}{\tau_g} \right) E_{cav} + \sqrt{\frac{1}{\tau_c}} E_{in}$$

where ω_0 is the field pulsation at resonance, $\frac{1}{\tau_g}$ the gain term and $\tau_{0,c} = \frac{2Q_{0,c}}{\omega_0}$. When the gain material is composed of QWs embedded in a semiconductor slab, this term depends on the carrier density [29] as follows: $\frac{1}{\tau_g} = \frac{\Gamma}{2} \sigma v_g (N - N_{tr})$ with Γ the confinement factor, σ the differential gain, v_g the light group velocity and N_{tr} the carrier density at transparency. The transmission can then be expressed as:

$$T(\omega) = \left| 1 - \frac{\frac{1}{\tau_c}}{j(\omega - \omega_0) + \frac{1}{\tau_c} + \frac{1}{\tau_0} - \frac{1}{\tau_g}} \right|^2$$

Fig. 3c shows the theoretical transmission at resonance $T(\omega_0)$ as a function of $\frac{1}{\tau_g}$ for $Q_0=10000$

and $Q_c=2000$, i.e. with a ratio Q_0/Q_c of 5. When $\frac{1}{\tau_g}$ is negative, the material is absorptive and the transmission stays close to 1. As $\frac{1}{\tau_g}$ is increased and becomes positive, the transmission diminishes

and falls to zero when the gain compensates exactly the intrinsic losses of the cavity ($\frac{1}{\tau_g} = \frac{1}{\tau_0}$). For this gain, the total cavity losses are determined by the coupling to the SOI waveguide and Q_c can be directly obtained by measuring the FWHM of the resonance in the transmission spectrum. When $\frac{1}{\tau_g}$

is further increased, net amplification is observed for $\frac{1}{\tau_g} > \frac{1}{\tau_0} + \frac{1}{2\tau_c}$ and laser threshold is reached

when $\frac{1}{\tau_g} = \frac{1}{\tau_0} + \frac{1}{\tau_c}$ (gain compensates all losses).

Pump-probe experiments are performed to measure the variation of the transmission spectrum around the cavity resonance wavelength as a function of the gain material. The pump, again delivered by a 800nm modulated laser diode (40ns pulses at 300kHz repetition rate), controls the gain of the active material. A modulated tunable laser source around 1.5 μm (13ns pulses at 300kHz repetition rate) is injected in the SOI waveguide and used as the probe. An extra 5kHz modulation is applied to it in order to perform homodyne detection to discriminate the probe signal from the emission.

The measured transmission spectra are plotted in Fig. 4a as a function of the absorbed pump power for a cavity coupled to a 350nm wide waveguide. The transmission firstly deepens more and more at resonance as the pump power is increased and reaches a minimum at $\lambda=1550\text{nm}$ when $P_{\text{pump}}=P_0=12.4\mu\text{W}$. Net amplification is then observed before reaching the laser emission threshold estimated at 29.6 μW . Due to the dependence of the material refractive index on the carrier density, the change in amplitude is also accompanied by a blue-shift of the resonant wavelength which is clamped when the laser threshold is reached. The very good agreement of these measurements with modelling can be clearly appreciated in Fig. 4b, where the transmission at resonance is plotted as a function of the absorbed pump power. The FWHM of the resonance is measured to be 0.83nm at $P=P_0$ giving $Q_c=1800$ (see Fig. 4.c). These measurements are reproduced on samples containing low-n layers of different thickness (z) and III-V cavities coupled to Si waveguides of different widths (w). In order to evaluate the impact of these structure parameters on the evanescent wave coupling, the measured Q_c are plotted on Fig. 5a. As expected from theory [30], Q_c strongly increases with z for a fixed value of w as the evanescent tail of the field of each level rapidly decays with the distance. As w is varied, Q_c varies from 5000 to 32000, from 1500 to 7800, from 1400 to 3700 for $z=400\text{nm}$, $z=300\text{nm}$, $z=200\text{nm}$ respectively. For all z , a minimum is reached for $w=400\text{nm}$, a width corresponding to a propagating mode in the Si waveguide with an effective index of 2.3 matching the one of the InP-based wire where the cavity is etched. This effective index-matching condition enables the maximum transfer of light and thus the minimum Q_c .

The unloaded quality factor Q_0 is obtained by fitting the L-L curve with standard rate equations for QWs lasers [29]:

$$\frac{dS}{dt} = \frac{-S}{\tau_{\text{ph}}} + \Gamma\sigma v_g (N - N_{\text{tr}})S + \Gamma\beta BN^2$$

$$\frac{dN}{dt} = \frac{-N}{\tau_{\text{nr}}} - BN^2 + \sigma v_g (N - N_{\text{tr}})S + R$$

where S is the photon density, N the carrier density, τ_{ph} the photon lifetime, β the spontaneous emission factor, B the bimolecular radiative recombination coefficient, τ_{nr} the non-radiative carrier relaxation time and R the pumping rate proportional to the optical pump fluence. τ_{ph} is linked to τ_0 and τ_c by the relation $(\tau_{\text{ph}})^{-1} = 1/2((\tau_c)^{-1} + (\tau_0)^{-1})$. Γ and v_g are fixed to 0.25 and $10^8 \text{ m}\cdot\text{s}^{-1}$ values obtained from

3D FDTD calculations [19]. We take from the literature [31] $N_{tr}=10^{18}\text{cm}^{-3}$ and $B=3.10^{10}\text{cm}^3.\text{s}^{-1}$. T_{nr} is measured to be 200ps [32]. For the fitting, we add to the rate equations the last condition giving σ :

$$\sigma = \frac{2}{\Gamma_{vg} N_{tr}} \left(\frac{1}{\tau_c} \frac{P_0}{2(P_1 - P_0)} - \frac{1}{\tau_0} \right)$$

where P_1 is the pump power when the transmission at resonance equals to 1. β is let as a free variable. The result of the fit using this model is plotted on Fig. 2a together with the measurements. Excellent fits of the measurements are obtained for τ_0 ranging from 10ps to 83ps ($6100 < Q_0 < 50000$) and $0.16 < \beta < 0.35$. In order to sharpen the estimations, these values are cross-checked with the results of the fit of a L-L curve for the same cavity but coupled to a waveguide of different width. We obtain $16.5\text{ps} < \tau_0 < 49.5\text{ps}$ ($10000 < Q_0 < 30000$) and $0.2 < \beta < 0.3$ which are typical values for this type of nanolasers allowing low laser threshold and ultrafast dynamics [33]. Even though a precise value of τ_0 can't be determined, this method is preferred to the usual way of finding the Q factor which consists in measuring the laser spectral linewidth at threshold as the linewidth of a semiconductor laser is not simply fixed by the optical losses in the system but depends on the pump duration, the phase-amplitude coupling and the different noise sources [34]. However, our results give us sufficient insight on the total losses of the system to determine the coupling efficiencies of the nanolasers to the SOI wires. The coupling efficiency, η , of the emitted light into the Si wires is plotted for the different studied structures in Fig. 5b. Each segment represents the possible range of values for η taking into account the uncertainties on Q_0 . By adjusting the parameters of the structures we demonstrate it is possible to tune this efficiency at will from around 20% to more than 90% by controlling the evanescent wave coupling strength, i.e. Q_c . As expected, the maximum of efficiency is obtained for the thinnest low-n layer and for $w=400\text{nm}$ which gives the smallest value of Q_c . Yet, the cases corresponding to the highest η do not necessarily correspond to the ideal configuration as it also gives the largest optical losses in the system which may result in an increase of the laser threshold or worse in a non-lasing situation. The transition from lasing to non-lasing structures is observed to occur when the coupling efficiency goes beyond 88%. This estimated boundary between the two regimes is indicated by the dotted line on Fig. 5b. It shows that, for the ensemble of fabricated structures, approximately 88% of laser emission may be coupled into a single mode SOI wire.

Conclusion and Discussion:

The concept of hybrid III-V semiconductor/silicon photonics has been brought forward to nanophotonics by the integration of InP-based PhC nanolasers on SOI single mode waveguides. We have demonstrated the most compact lasers integrated on a Si optical circuitry with low thresholds and within the telecom window. This system has many assets both in the performance as well as for the future applications. Indeed, taking advantage of the quasi perfect confinement of light within PhCs, we have fabricated lasers with $5\mu\text{m}^2$ footprints corresponding to at least a 10 times improvement over currently demonstrated hybrid systems. The breakthrough result in this work is that almost all the emitted light is useful as it is efficiently coupled the subjacent Si waveguides and can be further used

in a directly CMOS compatible dense nanophotonic networks of interconnects adapted for computer-com.

The highly efficient evanescent wave coupling was obtained by tailoring the optical properties of both the SOI waveguide and the III-V nanocavity and through a fine control over the technological processing of the structure.

Up to now, the practical use of PhCs in integrated photonic circuit has been an extremely challenging task. Establishing the communication between active nanodevices and the outside world, while mastering optical losses and photonic functionalities has, indeed, been one of the major problems. To the best of our knowledge, two solutions have been proposed in literature: the first one consists in using a tapered optical fibre to extract the light from the PhC [35,36]. This approach, obviously limited to one isolated element presents also limitations in terms of coupling due to the large difference in refractive indices between the optical fibre and the III-V semiconductor. The other possibility is an all III-V semiconductor based approach as for telecom devices, making use of epitaxial regrowth to separate the active regions where the lasers are made from the passive ones where light propagates without being absorbed [37]. Compared to the hybrid approach, this type of structures suffers from the lack of direct compatibility with CMOS electronics as they are made in a different platform. Moreover, the all III-V semiconductor solution relies on the use of suspended membranes to form the high index contrast waveguide necessary for the vertical confinement when PhC are evoked which is an evident drawback for mechanical reliability. The III-V/SOI hybrid system brings an efficient and elegant solution for making use of active PhCs within a photonic circuit combining the best of III-V semiconductor and Si photonics.

The last obstacle preventing the use of PhC nanolasers with electronics is now the electrical injection which is necessary for making an electro-optical conversion. Recent progress on this subject consisting in either achieving a lateral PIN junction [39] or a smart design of the electrical contacts [40] are encouraging approaches which could be implemented also within our hybrid system.

METHOD

Fabrication of the III-V/SOI hybrid nanolasers

The fabrication of the hybrid structures relies on the adhesive bonding using Benzocyclobutene (BCB) of the MOCVD grown InP-based heterostructure containing the active membrane on the SOI wafer processed with the waveguides of interest in a CMOS pilot-line. A 300nm thick layer of BCB is spun onto the SOI wafer surface in order to planarise the surface and let 80nm of polymer above the Si waveguides. The InP wafer is coated with a SiO₂ layer whose thickness is chosen to be 200nm, 300nm or 400nm before being put in contact with the SOI wafer coated with BCB. The sample is then pressed and cured for 3 hours at 300°C under N₂ atmosphere to finalise the bonding. After the chemical removal of the InP substrate, the PhC cavities are patterned in the active membrane using inductively coupled plasma etching through a silicon nitride mask obtained by electron beam lithography followed by reactive ion etching. A 30nm-precise alignment of the III-V nanocavities to the SOI waveguides is achieved by using during the electron beam lithography reference markers fabricated in the SOI level. After the silicon nitride mask removal, the undesired extra InP-based membrane left on the surface is chemically etched away while protecting the nanocavities with a polymer patterned in a step of negative electron beam lithography. More details on the fabrication can be found in references [22].

References

- [1] M. J. Koblinsky, B. A. Block, J.-F. Zheng, B. C. Barnett, E. Mohammed, M. Reshotko, F. Robertson, S. List, I. Young, and K. Cadien, On-chip optical interconnects, *Intel Technol. J.*, **8**,. 129–141 (2004).
- [2] G. Roelkens, L. Liu, D. Liang, R. Jones, A. Fang, B. Koch, J. Bowers, III-V/silicon photonics for on-chip and inter-chip optical interconnects, *Laser Photonics Rev.* **4**, 751–779 (2010)

- [3] D. A. B. Miller, Physical reasons for optical interconnection, *Int'l J. Optoelectronics* **11**, 155-168 (1997).
- [4] P. Dumon, W. Bogaerts, V. Wiaux, J. Wouters, S. Beckx, J. Van Campenhout, D. Taillaert, B. Luyssaert, P. Bienstman, D. Van Thourhout, and R. Baets, Low-loss SOI photonic wires and ring resonators fabricated with deep UV lithography, *IEEE Photonics Technol. Lett.* **16**, 1328 (2004).
- [5] Y. Vlasov, S. McNab, Losses in single-mode silicon-on-insulator strip waveguides and bends, *Opt. Express* **12**, 1622-1631 (2004).
- [6] A. W. Fang, H. Park, O. Cohen, R. Jones, M. J. Paniccia, and J. E. Bowers, Electrically pumped hybrid AlGaInAs-silicon evanescent laser, *Opt. Express* **14**, 9203-9210 (2006).
- [7] J. Van Campenhout, P. Rojo Romeo, P. Regreny, C. Seassal, D. Van Thourhout, S. Verstuyft, L. Di Cioccio, J. -M. Fedeli, C. Lagae, and R. Baets, "Electrically pumped InP-based microdisk lasers integrated with a nanophotonic silicon-on-insulator waveguide circuit, *Opt. Express* **15**, 6744-6749 (2007).
- [8] A. W. Fang, E. Lively, Y.-H. Kuo, D. Liang, J. E. Bowers, A distributed feedback silicon evanescent laser, *Opt. Express* **16**, 4413-4419 (2008).
- [9] T. Dupont, L. Grenouillet, A. Chelnokov, and P. Viktorovitch, Contradirectional Coupling Between III-V Stacks and Silicon-On-Insulator Corrugated Waveguides for Laser Emission by Distributed Feedback Effect, *IEEE Photon. Tech. Lett.* **22**, 1413-1415 (2010).
- [10] H. Park, A. W. Fang, O. Cohen, R. Jones, M. J. Paniccia, J. E. Bowers, A Hybrid AlGaInAs–Silicon Evanescent Amplifier *IEEE Photon. Technol. Lett.* **19**, 230-2232 (2007).
- [11] H.-W. Chen, Y.-H. Kuo, and J. E. Bowers, High speed hybrid silicon evanescent Mach-Zehnder modulator and switch, *Opt. Express* **16**, 20571-20576 (2008)
- [12] L. Liu, J. Van Campenhout, G. Roelkens, Richard A. Soref, D. Van Thourhout, P. Rojo-Romeo, P. Regreny, C. Seassal, J.-M. Fédéli, R. Baets, Carrier-injection-based electro-optic modulator on silicon-on-insulator with a heterogeneously integrated III-V microdisk cavity, *Opt Letters* **33**, .2518-2520 (2008).
- [13] L. Liu, R. Kumar, K. Huybrechts, T. Spuesens, G. Roelkens, E.-J. Geluk, T. de Vries, P. Regreny, D. V. Thourhout, R. Baets and G. Morthier, An ultra-small, low-power, all-optical flip-flop memory on a silicon chip, *Nature Photon.* **4**, 18 -187 (2010).
- [14] H. A. Haus, *Waves and Fields in Optoelectronics*. Englewood Cliffs, NJ. Prentice-Hall (1984).
- [15] J. S. Foresi, P. R. Villeneuve, J. Ferrera, E. R. Thoen, G. Steinmeyer, S. Fan, J. D. Joannopoulos, L. C. Kimerling, Henry I. Smith, and E. P. Ippen, Photonic-bandgap microcavities in optical waveguides, *Nature* **390**, 143-145(1997).
- [16] A. R. Md Zain, N. P. Johnson, M. Sorel, and R. M. De La Rue, Ultra high quality factor one dimensional photonic crystal/photonic wire micro-cavities in silicon-on-insulator (SOI), *Opt. Express* **16**, 12084–12089 (2008).
- [17] P. B. Deotare, M. W. McCutcheon, I. W. Frank, M. Khan, and M. Lončar, High quality factor photonic crystal nanobeam cavities, *Appl. Phys. Lett.* **94**, 121106 (2009).
- [18] Y. Gong, B. Ellis, G. Shambat, T. Sarmiento, J. S. Harris, and J. Vuckovic, Nanobeam photonic crystal cavity quantum dot laser, *Opt. Express* **18**, 8781–8789 (2010).
- [19] Y. Halioua, A. Bazin, P. Monnier, T. J. Karle, I. Sagnes, G. Roelkens, D. Van Thourhout, F. Raineri, and R. Raj, III-V photonic crystal wire cavity laser on silicon wafer, *J. Opt. Soc. Am. B*, **27**, 10 (2010).
- [20] P. Velha, J. C. Rodier, P. Lalanne, J. P. Hugonin, E. Picard, T. Charvolin, and E. Hadji, "Ultra-high-reflectivity photonic-bandgap mirrors in a ridge SOI waveguide," *New J. Phys.* **8**, 204 (2006).
- [21] B.-S. Song, S. Noda, T. Asano and Y. Akahane, Ultra-high-Q photonic double-heterostructure nanocavity, *Nature Mat.* **4**, 207-210 (2005).
- [22] T. J. Karle, Y. Halioua, F. Raineri, P. Monnier, R. Braive, L. Le Gratiet, G. Beaudoin, I. Sagnes, G. Roelkens, F. van Laere, D. Van Thourhout, and R. Raj, Heterogeneous integration and precise alignment of InP-based photonic crystal lasers to complementary metal-oxide semiconductor fabricated silicon-on-insulator wire waveguides, *J. Appl. Phys.* **107**, 063103 (2010).
- [23] G. Bjork and Y. Yamamoto, Analysis of semiconductor microcavity lasers using rate equations, *IEEE J. Quantum Electron.* **27**, 2386–2396 (1991).
- [24] E. Kapon, *Semiconductor Lasers*, Academic, New York, 1999.
- [25] M. Schmid, S. Benchabane, F. Torabi-Goudarzi, R. Abram, A. I. Ferguson, and E. Riis, Optical in-well pumping of a vertical-external-cavity surface-emitting laser, *Appl. Phys. Lett.* **84**, 4860 (2004).

- [26] W. Suh, Z. Wang, S. Fan, Temporal coupled-mode theory and the presence of non orthogonal modes in lossless multimode cavities, *IEEE J. Quant. Elec.* **40**, 1511-18 (2004).
- [27] C. Manolatou, M. J. Khan, S. Fan, P.R. Villeneuve, H. A. Haus, and J. D. Joannopoulos, Coupling of Modes Analysis of Resonant Channel Add-Drop Filters, *IEEE J. Quant. Elec.* **35**, 9 (1999).
- [28] Y. Dumeige, S. Trebaol, L. Ghis, T.K.N. Nguyễn, H. Tavernier, and P. Féron, Determination of coupling regime of high-Q resonators and optical gain of highly selective amplifiers, *J. Opt. Soc. Am. B* **25**, 12 (2008).
- [29] P. S. Zory, *Quantum well Lasers*, Academic, San Diego California, 1993.
- [30] W.-P. Huang, Coupled-mode theory for optical waveguides : An overview, *J. Opt. Soc. Am. A* **11**, 963-983 (1994).
- [31] H. Kawaguchi, Optical bistability and chaos in a semiconductor laser with saturable absorber, *Appl. Phys. Lett.* **45**, 1264-1266 (1984).
- [32] F. Raineri, C. Cojocaru, P. Monnier, A. Levenson, R. Raj, C. Seassal, X. Letartre, and P. Viktorovitch, Ultrafast dynamics of the third-order nonlinear response in a two-dimensional InP-based photonic crystal, *App. Phys. Lett.* **85**, 1880-1882 (2004).
- [33] H. Altug, D. Englund, and J. Vuckovic, Ultrafast photonic crystal nanocavity laser, *Nature Phys.* **2**, 484-488 (2006).
- [34] E. Rosencher and B. Vinter, *Optoelectronics*, Cambridge University Press, Cambridge UK, 2002.
- [35] P. E. Barclay, K. Srinivasan, and O. Painter, Design of photonic crystal waveguides for evanescent coupling to optical fiber tapers and integration with high-Q cavities, *J. Opt. Soc. Am. B* **20**, 2274-2284 (2003).
- [36] I.-K. Hwang, S.-K. Kim, J.-K. Yang, S.-H. Kim, S. H. Lee, and Y.-H. Lee, Curved-microfiber photon coupling for photonic crystal light emitter, *Appl. Phys. Lett.* **87**, 131107 (2005)
- [37] K. Nozaki, H. Watanabe, and T. Baba, Photonic crystal nanolaser monolithically integrated with passive waveguide for effective light extraction, *Appl. Phys. Lett.* **92**, 021108 (2008).
- [38] S. Matsuo, A. Shinya, T. Kakitsuka, K. Nozaki, T. Segawa, T. Sato, Y. Kawaguchi, M. Notomi, High-speed ultracompact buried heterostructure photonic-crystal laser with 13fJ of energy consumed per bit transmitted, *Nature Photon.* **4**, 648-654 (2010)
- [39] B. Ellis, T. Sarmiento, M. Mayer, B. Zhang, J. Harris, E. Haller, and J. Vuckovic, *Applied Physics Letters*, **96**, 181103 (2010).
- [40] H.-G. Park, S.-H. Kim, S.-H. Kwon, Y.-G. Ju, J.-K. Yang, J.-H. Baek, S.-B. Kim, and Y.-H. Lee, Electrically Driven Single-Cell Photonic Crystal Laser, *Science* **305**, 1444-1447 (2004).

Acknowledgements

The authors acknowledge for funding FP7 HISTORIC European Project and ANR Jeunes chercheurs French National project PROWOC. The SOI wafers were fabricated within the ePIXfab European silicon platform. We thank Remy Braive for his help in the etching of photonic crystals and Bjorn Maes for useful discussion.

Author contributions

A.B. and Y. H. contributed equally to make this work successful and would both deserve to be first author. A.B., Y.H., I.S. and F.R. fabricated the structures under study. A.B., Y.H., F.R., P.M and R.R. carried out the measurements. A.B., Y.H. and F.R. analysed the measurements. Y.H. proposed and designed the wire cavity photonic crystal structures. T.K. designed the SOI waveguide circuitry. A.B. and F.R. wrote the article. G.R. supervised this study at Ghent University. R.R. and F.R. proposed the study of hybrid structures for nanophotonics and coordinated the entire work.

Figure Captions

Figure 1 Hybrid III-V Semiconductor Photonic Crystal on SOI waveguide circuitry. **a**, Schematic view of the structure. The InP-based photonic-crystal wire cavity nanolaser is positioned on top of silicon on insulator strip waveguide. The 2 structures are separated by a low-refractive index bonding layer constituted of BCB and SiO₂. **b**, SEM images of the fabricated sample. The SOI waveguides can be seen through the bonding layer aligned with the cavities. Inset: SEM image close-up of a wire cavity.

Figure 2 Experimental PhC wire cavity nanolaser emission characteristic curves. **a**, Intensity of the emitted light outputting the SOI waveguide as a function the absorbed pump power. The black line is a fit of the experimental data using the rate equations for quantum well lasers given in the text. **b**, Full width at half maximum of the emission spectral linewidth as a function of the absorbed pump power. **c**, Emission wavelength as a function of the cavity length, i.e. the distance centre to centre between the first 2 tapered holes. Laser operation is observed to be single-mode for cavity lengths under 550 nm.

Figure 3 Coupling model. **a**, Theoretical coupling efficiency as a function of the ratio Q_0/Q_c . **b**, Schematics of the system considered for the couple mode theory. An incoming field E_{in} in the SOI waveguide is coupled to a single mode cavity via evanescent wave coupling. The intracavity field is denoted E_{cav} and the transmitted field in the forward direction $E_{out\ forward}$. $(\tau_0)^{-1}$ and $(\tau_c)^{-1}$ are the inverse of the time constants corresponding to the intrinsic losses of the cavity and to the coupling between the cavity and the waveguide. The presence of the active material in the cavity is taken into account by adding an extra characteristic time constant τ_g which depends on the absorption/gain of the material. **c**, Theoretical transmission at resonance as a function of $(\tau_g/\tau_0)^{-1}$ for $Q_0/Q_c=5$ obtained with couple mode theory. A minimum is reach for $\tau_g=\tau_0$ and the laser threshold is reached for $(\tau_g^{-1})=(\tau_0)^{-1}+(\tau_c)^{-1}$, i.e. in the chosen case for $(\tau_g/\tau_0)^{-1}=6$.

Figure 4 Experimental transmission results. **a**, Transmission spectra of the coupled system as a function of the absorbed pump power. These measurements are carried out using a laser source tunable between 1.5 μ m and 1.6 μ m which is injected into a Si waveguide coupled to a wire cavity laser pumped by a 800nm laser diode. A Blue-shift of the resonance is observed due to the index change produced the increase of the carrier density. Above 19 μ W of pump power, net gain is observed. Laser threshold is reached at a pump power at nearly 30 μ W (outside the data range). **b**, Transmission at resonance as a function of the pump power, these values corresponding to transmission minimum/maximum when the spectra exhibit a dip/peak. The shape of the obtained is in good agreement with the modelling (cf. Fig 3c) **c**, Transmission spectrum obtained with a 12.4 μ W pump power corresponding to the case when $\tau_g=\tau_0$ giving the minimum of transmission at resonance. The fitting of the curve using a lorentzian lineshape gives a FWHM of 0.83nm.

Figure 5 Characteristic coupling figures. **a**, Measured quality factor associated to the evanescent wave coupling (Q_c) for various SOI waveguide width w and for 3 low-index layer thicknesses. These values are deduced from the measurement of the FWHM of the cavity resonance when the pump power is fixed to have $\tau_g=\tau_0$. A minimum of quality factor (maximum of coupling efficiency, cf Fig. 5b) is observed for $w=400$ nm when phase-matching between the waveguide mode and the cavity mode occurs. **b** Coupling efficiency of the emitted light into the SOI wire as a function of the structure parameters. The coupling efficiency is obtained from the Q_c and Q_0 measurements, the latter being deduced from the laser characteristic curve fitted with the rate equations model (see Fig2.a). Given the range of the possible values for Q_0 , an uncertainty on the coupling efficiency is found and materialised the segments on the figure. We indicate by the black dotted line the estimated boundary in terms of coupling efficiency between lasing and non lasing structures.

Figure 1

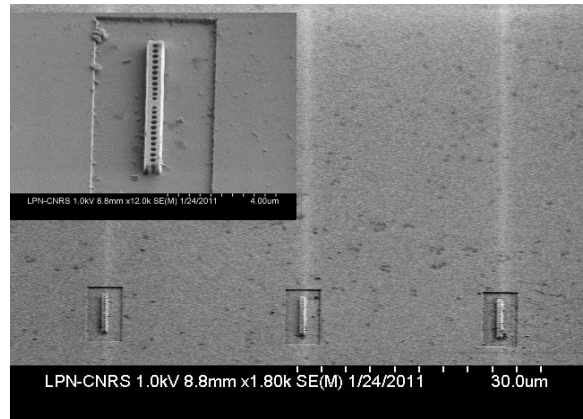
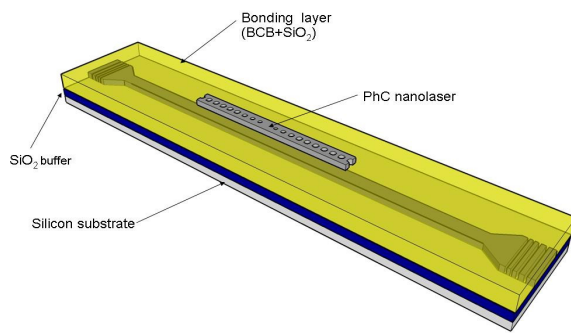


Figure 2

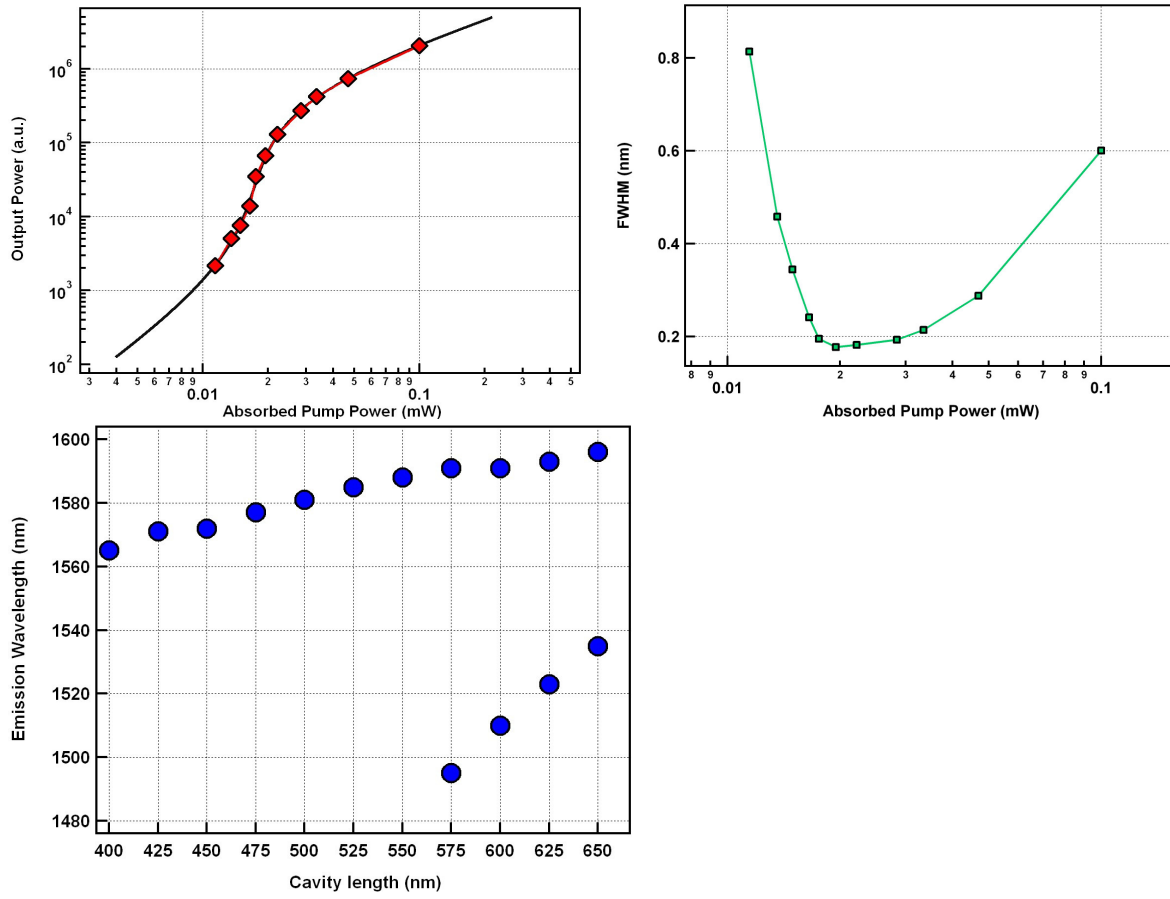


Figure 3

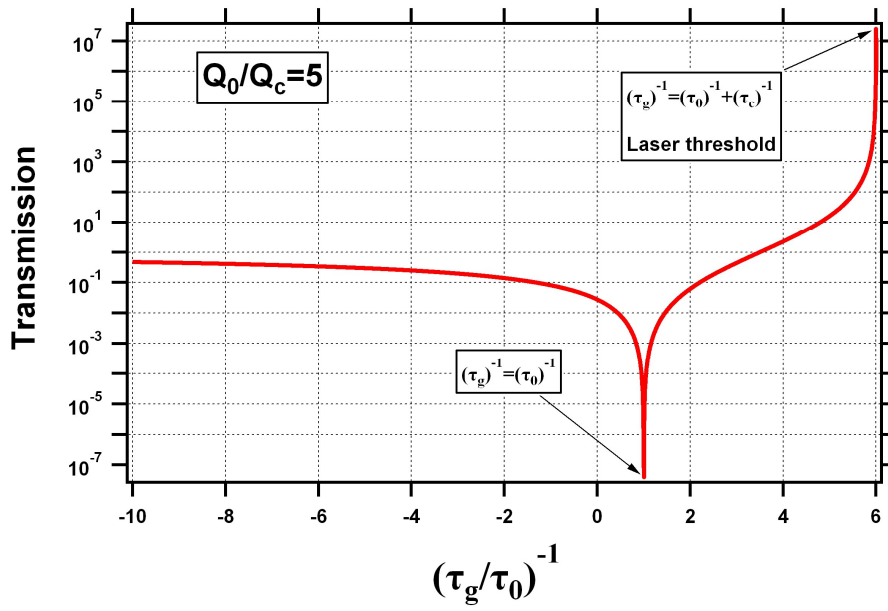
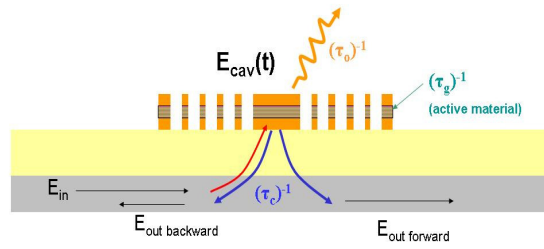
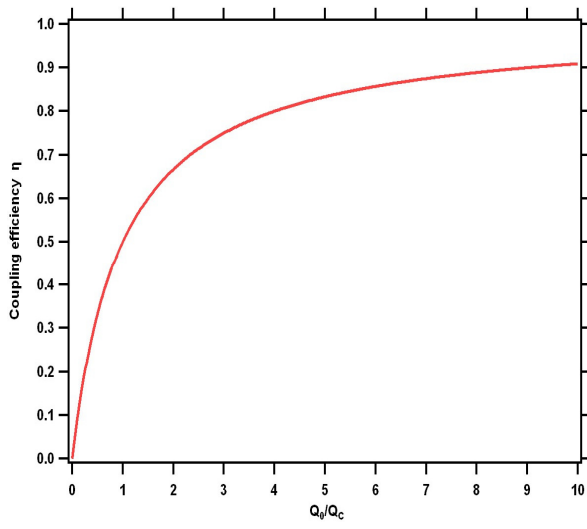


Figure 4

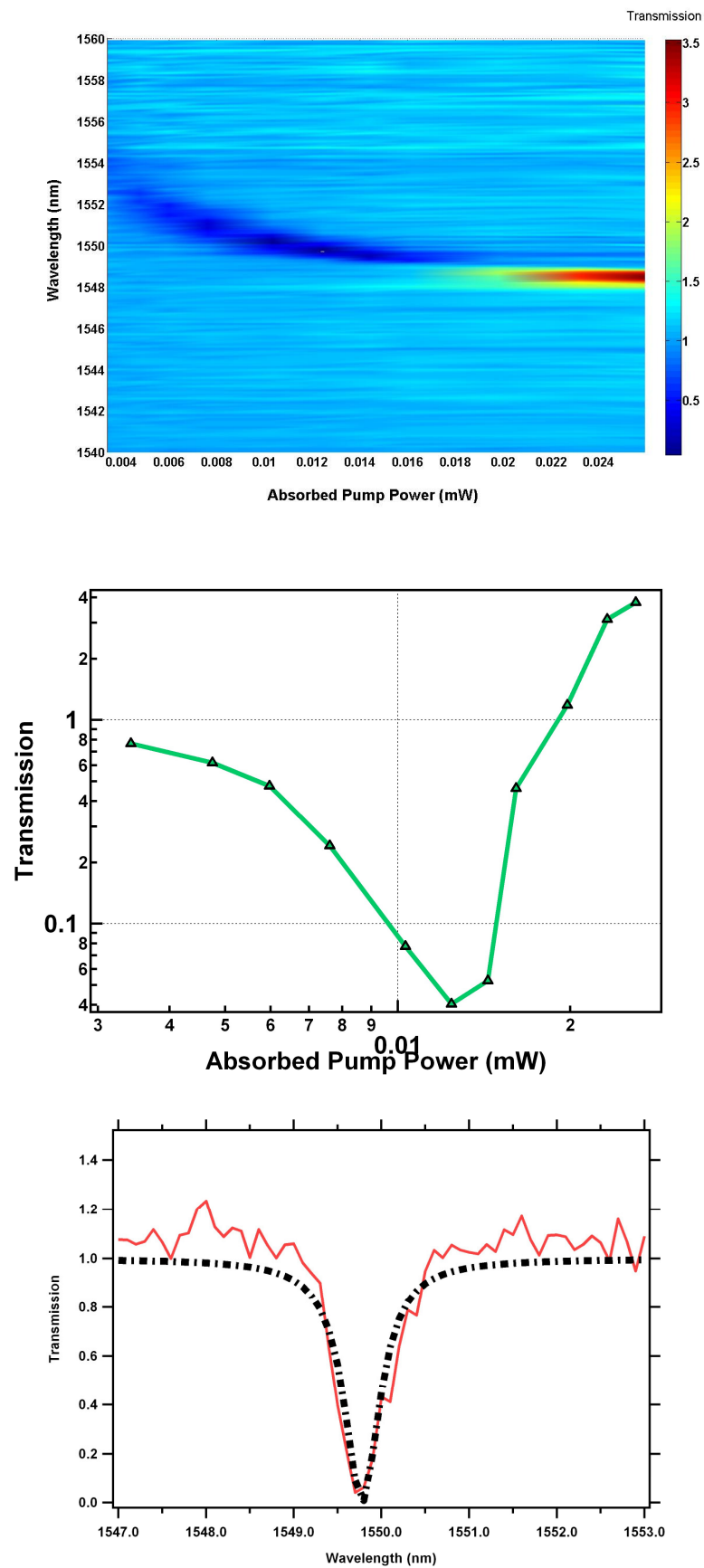


Figure 5

